IEEE Access
Multidisciplinary | Rapid Review | Open Access Journal

Received May 29, 2019, accepted June 23, 2019, date of publication June 27, 2019, date of current version July 16, 2019.

Digital Object Identifier 10.1109/ACCESS.2019.2925427

Three-Dimensional Numerical Simulation of Rock Breaking by the Tipped Hob Cutter Based on Explicit Finite Element

XIUKUN HU[1,2], CHANGLONG DU[1], SONGYONG LIU[1], HAO TAN[3,4], AND ZHIQIANG LIU[3,4]

[1]School of Mechatronic Engineering, China University of Mining and Technology, Xuzhou 221116, China
[2]Shandong Tai'an Coal Mining Machinery Company, Ltd., Tai'an 271000, China
[3]Institute of Mine Construction, Tiandi Science & Technology Company, Ltd., Beijing 100013, China
[4]National Engineering Laboratory for Deep Coal Construction Technology in Coal Mines, Beijing 100013, China

Corresponding author: Xiukun Hu (huxiukun2006@126.com)

This work was supported in part by the National Natural Science Foundation of Jiangsu Province under Grant BK20160250, and in part by the Priority Academic Program Development of Jiangsu Higher Education Institute of China.

ABSTRACT As an important equipment for wellbore construction, the raise boring machine (RBM) has been widely used in subway tunnels and mine construction projects. Its tipped hob cutter for rock breaking is directly related to the cost, safety, and overall performance of the project. However, few open studies research on the rock-breaking by the tipped hob cutter, and there is still a lack of enough understanding of how the cutter breaks rock and the form of the rock breaking. In this paper, we study how the tipped hob cutter breaks the rock, and how to establish the finite-element model of the rock breaking by the cutter, with using the numerical simulation software LS-DYNA to analyze the rolling process and rock fracture form of the cutter. By studying the fracture morphology of rocks, it is proposed that there are three fracture modes of rock breaking: forward slip, no slip, and backward slip, using the experimental verification. On this basis, study the variation laws and correlations of feed force, lateral force, and positive force under different moving speeds and penetration depths. The results in this paper can provide a theoretical basis for improving the tool design of the tipped hob cutter on the RBM against the efficiency of rock-breaking.

INDEX TERMS Tipped hob cutter, raise boring machine, rock fragmentation, slip crushing, numerical simulation.

I. INTRODUCTION

The 21st century is known as the underground engineering century, because the human beings need to build a lot of underground engineering structures to expand the utilization of space resources. As an important equipment for wellbore construction, the raise boring machine (RBM) have been widely used in mineral development, subway tunnels, urban pipe corridors, etc., so efficient construction of wells is particularly important. The RBM uses tipped hob cutter to break rock by rolling. Compared with the early application of rock breaking methods such as impact and cutting, it is the most efficient and adaptable rock breaking method [1]. Its working principle is that the drill pipe applies the tension to press the tipped hob cutter into the rock, and then the drill pipe rotates to drive the cutter to break the rock. The Figure 1 shows the structure of the cutterhead. The tipped hob cutter is arranged on the cutterhead in a certain way. In the process of the cutterhead rotation, the teeth of the tipped hob apply shearing and crushing to achieve rock damage. The Figure 2 shows the rock-breaking model of the tipped hob cutter whose teeth generate cracks on the rock, which will cause the rock to break.

At present, the researchers mainly study the disc hob on the tunnel boring machine (TBM), which is very similar in shape and function to the tipped hob cutter [2]. In the analysis using the finite element method, the force of the disc hob in all directions and how to determine the optimal cutting pitch are mainly studied [2]–[8]. The main purpose of the research is to improve the design of the disc hob and the cutter head.

In the analysis using the discrete element method, the effect of different disc hobs on the rock crushing effect is mainly studied, which is used to accurately describe various

The associate editor coordinating the review of this manuscript and approving it for publication was Jiansong Liu.

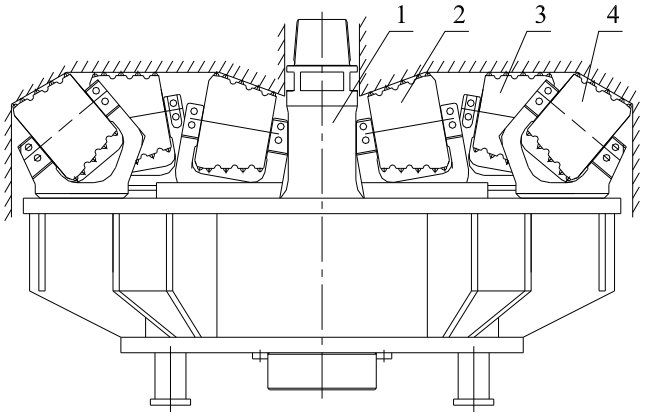

1. Drill pipe 2. Center cutter 3. Front cutter 4. Side cutter

FIGURE 1. Cutterhead structure of the raise boring machine.

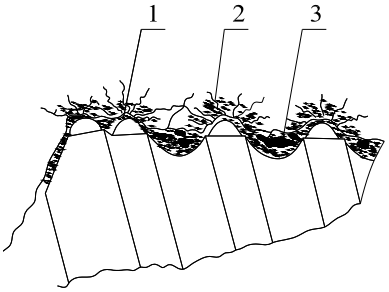

1. Crushed rock powder 2. Internal crack of rock 3. Rock fragment

FIGURE 2. Rock-breaking model of the tipped hob.

parameters of the rock and predict the force of the tools under different rocks [9]–[13]. Both the tipped hob and the disc hob are crushed by the cutter to break the rock, but unlike the disc hob which causes continuous damage on the rock surface, the tipped hob causes discontinuous damage. This means that the tipped hob and the disc hob are different in the mechanism of rock fracture, and further research on its mechanism is needed [14].

In the study of rock fragmentation, it is very suitable and effective to use the finite element method to simulate the rock breaking performance of different tools [15]–[20]. During rock fragmentation, the cutting force is not only affected by friction and cutting speed, but also by mechanical properties of the rock and tool angle [16], [17]. In the process of breaking hard rock, the increase of cutting force is the main cause of tool failure and low cutting efficiency [18]. In addition, The cutting forces and chip morphology were significantly influenced by sliding velocities and cutting depths [19], [20].

Related experiments have also shown that this method can accurately predict the force of the tool and achieve the rock crushing effect similar to the actual [6], [21], [22]. Compared with these cutters, there is no research on the rock breaking of the tipped hob on the raise boring machine. In this paper, the finite element is used to analyze the rock breaking of the tipped hob cutter, and further experiments are used to verify the simulation results, in order to prepare for the analysis of the crushing mechanism.

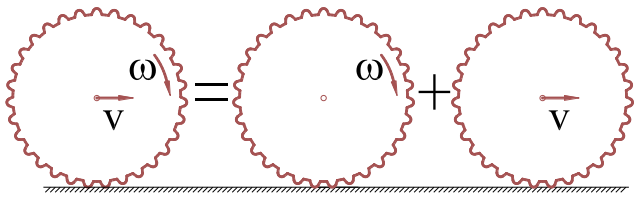

FIGURE 3. Decomposition of the tipped hob movement.

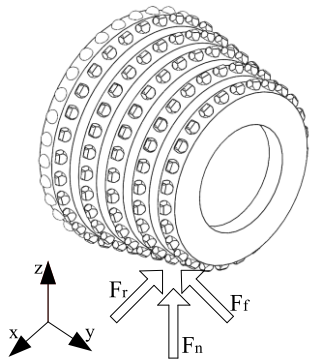

FIGURE 4. Force sketch of the tipped hob.

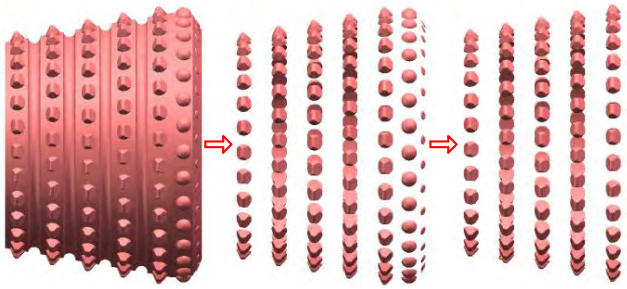

(a) A tipped hob cutter (b) Removing the body (c) Removing teeth

FIGURE 5. Simplification process of tipped hob cutter.

II. MODELS AND METHODS

A. PHYSICAL MODELS

In this paper, the failure modes of the hob at different rolling speeds are studied, and the variation law of the load in all of the hob's directions in the process of the rock breaking is explored, which is used as a reference for the design of a reasonable hob. In fact, the rolling motion of the hob cutter can be decomposed into two forms of the rotation motion and the translation motion, as shown in the Figure 3. The hob cutter will be subjected to three kinds of forces in the process of the rock breaking: positive force F_n, pointing to the broken rock surface and provided by the cutter head thrust; feed force F_r, pointing to the hob tangential direction and provided by the cutter wheel torque; lateral force F_f, pointing to the center of the cutterhead, which has the pressing force of the hob on the rock and the centrifugal force of the cutter disc rotation, as shown in the Figure 4.

To reduce the calculation time, the tipped hob cutter is simplified into regularly arranged teeth and the hob's rolling is transformed into rotary motion and translation motion. The Figure 5 is shows the simplified process of a tipped hob cutter.

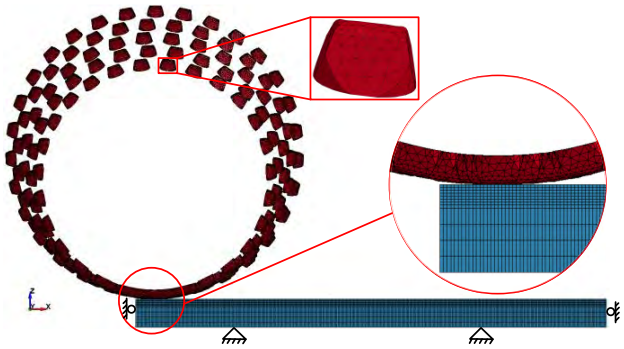

FIGURE 6. LS-DYNA model for simplified rock-breaking process of tipped hob cutter.

The rock is modeled as a cuboid with a length of 500 mm, a width of 200 mm and a thickness of 30 mm, and is meshed by a hexahedron with a number of units of 537,072 and 587,925 nodes. The finite element model is shown in the Figure 6.

Calculated by the rotation speed of the drill pipe at 5 rpm (0.5236 rad/s), the front cut rotates at a speed of 2.609 rad/s according to the position of the radius. The relative translation speeds of the cutter teeth corresponding to different radius are 345.69 mm/s, 356.13 mm/s, 373.09 mm/s, 391.35 mm/s, and 410.92 mm/s, respectively. In the numerical simulation, the angular velocity of the hob around the central axis is 2.609 rad/s, and the speed of the hob along the rock surface is set according to the five translation speeds mentioned above. In order to analyze the influence of different pressures on rock fragmentation, the depths of the rock erosion are set to 2 mm, 3 mm, 4 mm, 5 mm, and 6 mm respectively. The vibration and inclination of the hob in the process of rock breaking are not allowed, which limits the translation of the cutter body in the y-axis direction and the rotation around the x-axis and z-axis, and releases the rotation of the cutter body around the x-axis. In the contact model, the static and dynamic coefficients of friction were set to 0.45 and 0.4, respectively. The hob and the rock are in contact with the surface-to-surface erosion, and the bottom of the rock is completely constrained. The surrounding and bottom nodes of the rock are added with non-reflection boundary conditions to simulate the infinite boundary of the rock.

B. METHODS

In this paper, the explicit nonlinear finite element program LS-DYNA is used for numerical simulation. Assuming the rock is a homogeneous material, the presence of primary cracks and initial stress fields in the rock is not considered, and the rock is removed immediately after failure. This study does not care about the deformation and stress distribution of the cutter teeth, so the above assumptions have no effect on the results. All the cutter teeth are regarded as rigid bodies. The rigid body material model has a modulus of the elasticity of 600 GPa, a density of 14600 kg/m^3 and a poisson's ratio of 0.22. In the study, the rock material adopts bluestone. In order to reflect the rock fragmentation in the process of rolling the rock with the tipped hob cutter, the rock adopts the HJC (Holmquist-Johnson-Cook) model, which can describe the material in large strain and high strain. Defining the failure mode of rock as the shear strain failure. The HJC model mainly has three types of parameters: strength parameter, damage parameter and pressure parameter. Moreover, it includes state equation, yield surface equation and damage evolution equation.

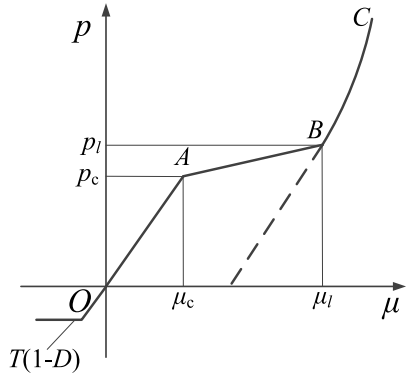

FIGURE 7. State equation.

The state equation, as shown in the Figure 7, mainly includes the stretching phase of the linear elastic region where only the damage factor and the linear elastic region ($p < p_c$) are considered, the plastic transition region ($p_c \le p \le p_l$), and the fully dense region ($p > p_l$). In the compression phase of the composition, the loading curve is expressed as follows:

$$p = \begin{cases} K_e\mu & p < p_c \\ p_c + K_c(\mu - \mu_c) & p_c \le p \le p_l \\ K_1\overline{\mu} + K_2\overline{\mu}^2 + K_3\overline{\mu}^3 & p \ge p_l \end{cases} \quad (1)$$

where, p, K_e and μ represent the hydrostatic pressure, bulk modulus and volume strain respectively; the hydrostatic pressure and the crushed volumetric strain at the elastic limit are represented by p_c and μ_c respectively; p_l and μ_l represent real-time pressure and volumetric strain respectively; K_1, K_2, and K_3 are material constants; $\overline{\mu}$ is corrected volumetric strain. Some of the physical quantities can be defined as:

$$K_e = p_c/\mu_c, \quad K_c = (p_l - p_c)/\mu_l - \mu_c, \ \overline{\mu} = \mu - \mu_l/1 + \mu_l$$

The yield surface equation of the HJC model, as shown in the Figure 8, can be expressed as:

$$\sigma^* = \left[A\,(1 - D) + Bp^{*N}\right]\left(1 + C\ln\dot{\varepsilon}^*\right) \quad (2)$$

where, $\sigma^* = \sigma/f_c'$ represents normalized equivalent stress; And σ, f', D represent actual equivalent stress, static compressive strength and damage degree ($0 \le D \le 1$); $p^* = p/f'c$ represents normalized hydrostatic stress; $\dot{\varepsilon}^* = \dot{\varepsilon}/\varepsilon_0$ represents dimensionless strain rate; $\dot{\varepsilon}$ represents actual strain rate; ε_0 represents reference strain rate; *A, B, C, N* are material constants.

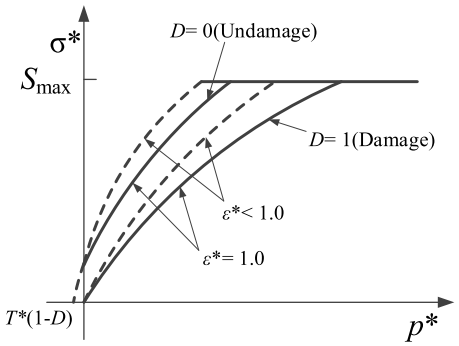

FIGURE 8. Yield surface equation.

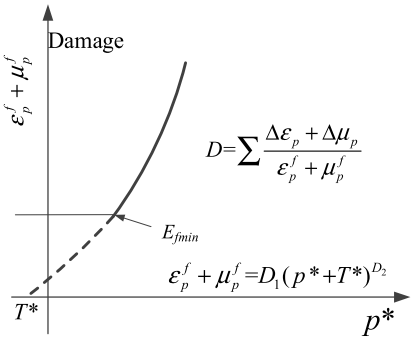

FIGURE 9. Damage evolution equation.

The HJC damage model is shown in the Figure 9. The damage is formed by the accumulation of equivalent plastic strain and plastic volumetric strain. The evolution equation is:

$$D = \sum \frac{\Delta\varepsilon_p + \Delta\mu_p}{\varepsilon_p^f + \mu_p^f} \tag{3}$$

$$\varepsilon_p^f + \mu_p^f = D_1(p* + T*)^{D_2} \tag{4}$$

where, $\Delta\varepsilon_p$ and $\Delta\mu_p$ represent equivalent plastic strain increment and plastic volume strain increment of the unit in the calculation cycle respectively; $\varepsilon_p^f + \mu_p^f$ represents plastic strain under the current integration step; $T^* = T/f_c'$ represents material normalized maximum tensile stress; T represents tensile strength; D_1 and D_2 are damage constants.

The rock is made of bluestone with a compressive strength of 122 MPa, which is the most common and representative material in the construction of the wellbore. The main parameters of the HJC model are shown in Table 1.

III. RESULTS AND DISCUSSION

A. SLIP PHENOMENON

As seen in the Figure 10, the damage of the rock by the tipped hob is discontinuous, and the crushing effect of the different rows of teeth on the rock is also different. In the process of breaking the rock, the rock will produce three different forms of damage due to the inconsistency between the translation speed and the rotation speed. In order to understand the difference in the fracture results, the broken fragments were sliced and analyzed.

TABLE 1. Material properties of a rock for simulation.

P (kg/m^3)	G (GPa)	A	B	C	N
2630	22.14	0.41	1.84	0.007	0.61
K_1 (GPa)	K_2 (GPa)	K_3 (GPa)	f'_c (MPa)	T (MPa)	p_c (MPa)
85	-171	208	122.3	9.5	41.43
μ_c	p_l (GPa)	μ_l	D_1	D_2	S_F
0.00192	0.9	0.04	0.04	1	15

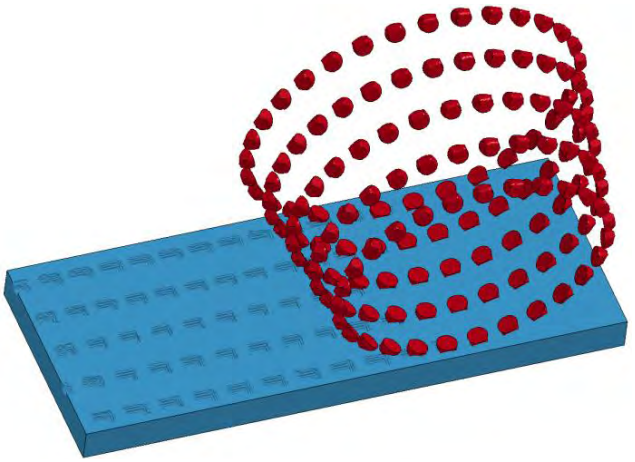

FIGURE 10. The results of rock breaking by the tipped hob cutter.

TABLE 2. Rock fracture states under different failure modes.

Failure form	1	2	3	4	5	6
Forward slip	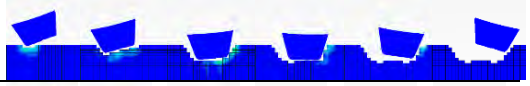					
No slip	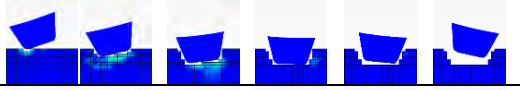					
Backward slid	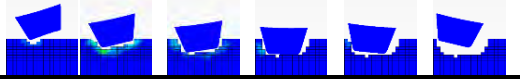					

1. When the translation speed of the hob is greater than the matching rotation speed, the failure form of the rock is defined as forward slip;

2. When the translation speed of the hob is equal to the matching rotation speed, the failure form of the rock is defined as no slip;

3. When the translation speed of the hob is less than the matching rotation speed, the failure form of the rock is defined as backward slid.

The Table 2 gives a detailed description of the movement process under the three failure modes. It can be seen the motion state of the cutter teeth relative to the rock is different, and the shape of the rock crater is also different, which are

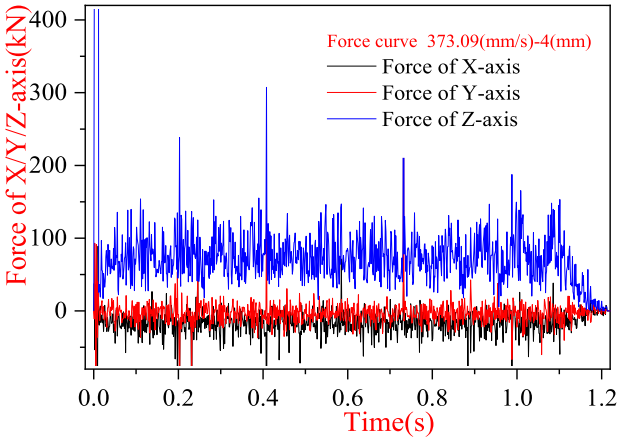

FIGURE 11. The force in the x/y/z directions of the tipped hob cutter.

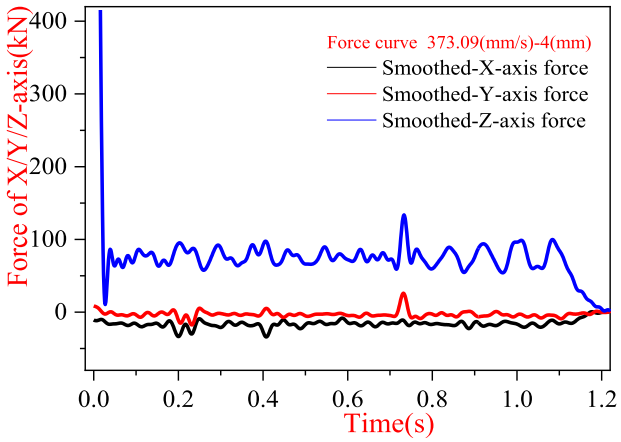

FIGURE 12. The force of the tipped hob cutter after smoothing in the x/y/z directions.

analyzed in the state of rock fragmentation, and further analysis of the force changes in the process of rock fragmentation is required.

B. CUTTING FORCE

The hob is subjected to forces in different directions in the process of the movement. These forces will constantly change due to the rock breaking state of the teeth, and this change has a periodicity. For the accuracy of the data, it is necessary to average the data in the period.

The Figure 11 is a plot of feed force, lateral force, and positive force as a function of time at a translation speed of 373.09 mm/s and in an erosion depth of 4 mm. It can be seen the obtained simulation results need to be smoothed to obtain a clearer curve. The Figure 12 is the smoothed curve as shown. According to the coordinate system established in the Figure 6, the results of the feed force and lateral force measurement are basically negative values. For the convenience of data analysis, the values of the feed force and the lateral force appearing in the subsequent graphs are all multiplied by −1. It can be seen the hob only has a large peak at the beginning of contact with the rock, and the rear always fluctuates within a small range. In the subsequent analysis of the data, the average value in the range of the middle 1s is used to average the force.

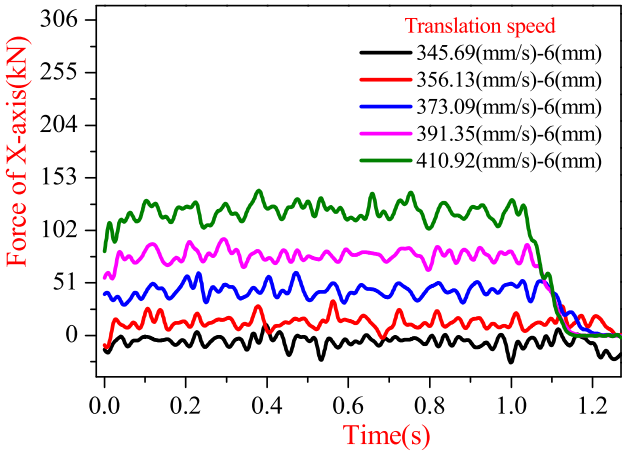

FIGURE 13. Feed force of the tipped hob cutter at different translation speeds.

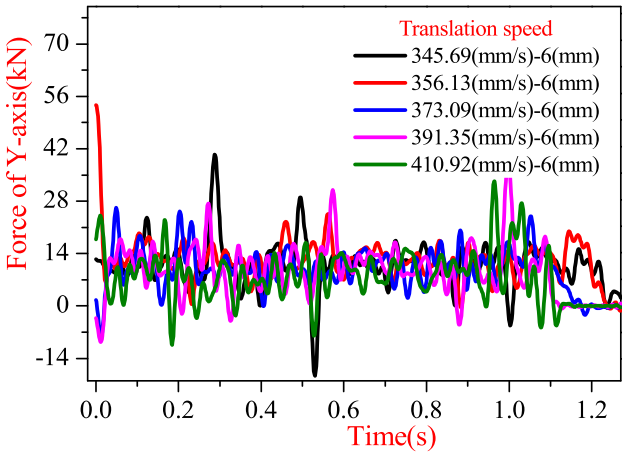

FIGURE 14. Lateral force of the tipped hob cutter at different translation speeds.

When the translation speed increases, the feed force and positive force of the hob increase, and the feed force has a negative value at the speed of 345.69 mm/s. At the same time, the peak-to-valley values of each group change at different speeds, indicating the feed force and positive force. The load fluctuations have periodicity, as shown in Figures 13 and 15, but the lateral force changes at different speeds are small, as shown in Figure 14.

With the following analysis of how the various parameters affect the feed force, lateral force and positive force of the hob, the results of numerical simulation are listed in the Table 3.

When the hob moves smoothly, the feed force increases significantly as the penetration depth and translation speed increase. Especially when the penetration depth increases, the feed force performance increases more prominently, as shown in the Figure 16 and Figure 17.

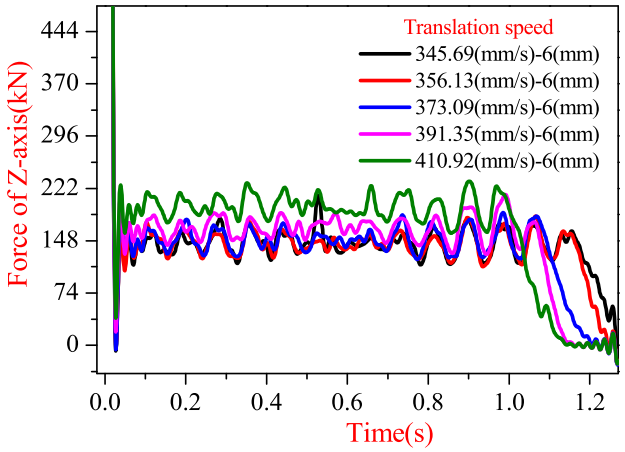

FIGURE 15. Positive force of the tipped hob cutter at different translation speeds.

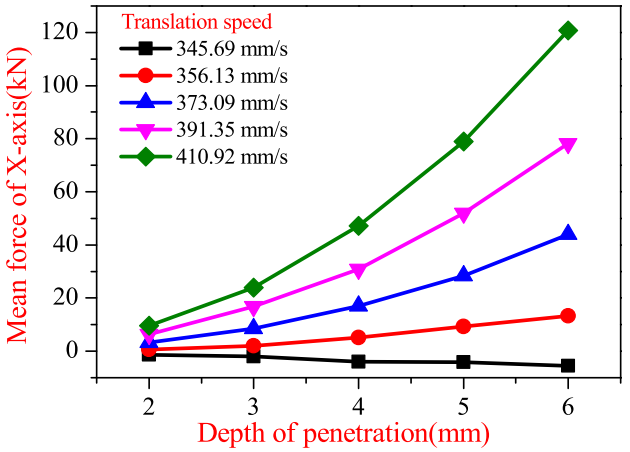

FIGURE 16. Feed force in different penetration depths.

TABLE 3. Results of X, Y, Z force and fracture volume.

Running speed (mm/s)	Penetration depth (mm)	Feeding force (kN)	Lateral force (kN)	Positive force (kN)	Crushing volume (cm^3)
345.69	2	1.35	0.57	22.50	12.89
	3	2.02	2.39	44.49	23.47
	4	3.92	4.08	74.47	36.77
	5	4.10	7.44	107.54	52.01
	6	5.52	11.49	144.97	69.25
356.13	2	0.70	1.31	22.57	12.70
	3	2.08	2.70	44.52	23.20
	4	5.18	4.65	73.12	35.95
	5	9.21	6.47	107.07	50.98
	6	13.32	12.23	144.35	67.88
373.09	2	3.28	0.45	21.95	12.13
	3	8.55	0.93	46.55	22.55
	4	16.96	3.20	76.40	35.14
	5	28.44	7.44	111.57	50.12
	6	43.91	11.07	149.76	67.36
391.35	2	6.36	0.78	25.41	12.74
	3	16.79	1.63	52.14	23.69
	4	30.81	3.00	85.11	37.09
	5	52.05	5.56	123.99	52.82
	6	78.25	10.41	166.44	70.97
410.92	2	9.55	0.52	29.05	13.42
	3	23.99	0.33	59.69	25.09
	4	47.25	1.60	97.77	39.57
	5	79.03	3.94	143.05	56.99
	6	120.82	8.41	196.30	77.27

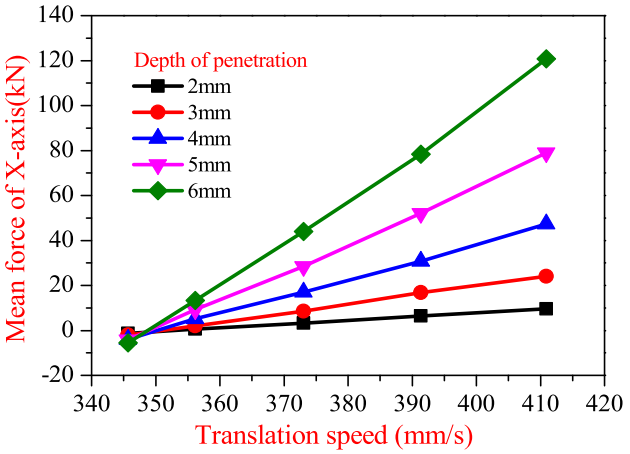

FIGURE 17. Feed force at different translation speeds.

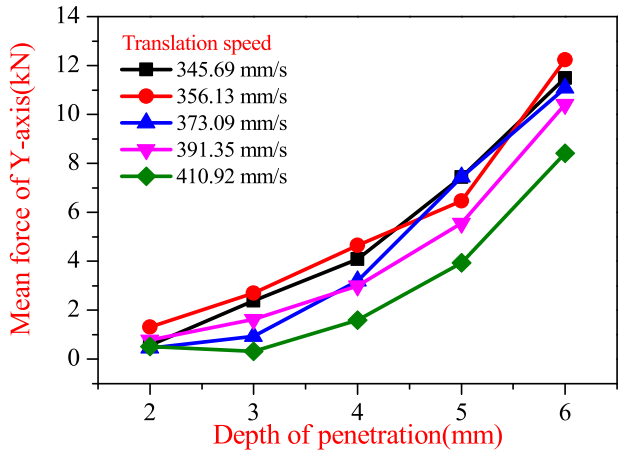

FIGURE 18. Lateral force in different penetration depths.

The lateral force increases as the penetration depth increases, and the variation trend basically remains the same at different translation speeds, as shown in the Figure 18. When the penetration depth is the same, the lateral force decreases as the translation speed increases, which indicates that the increase of the penetration depth effectively suppresses the lateral force, as shown in the Figure 19. Compared to the feed force, the hob lateral force value is much smaller.

The spacing between the curves in the Figure 20 increases as the hob translation speed increases, which indicates that as the hob penetration depth is constant, the positive force of the hob increases sharply as the translation speed

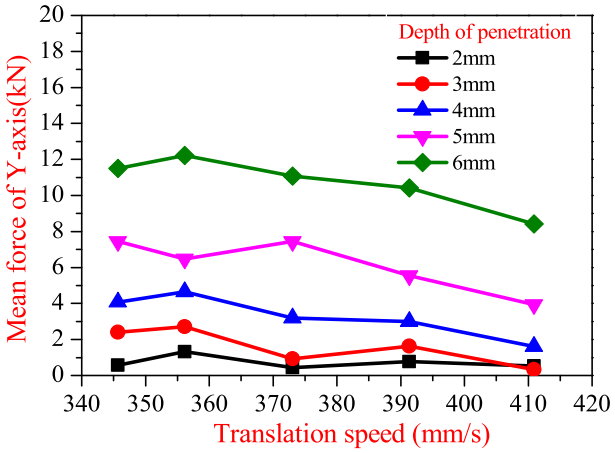

FIGURE 19. Lateral force at different translation speeds.

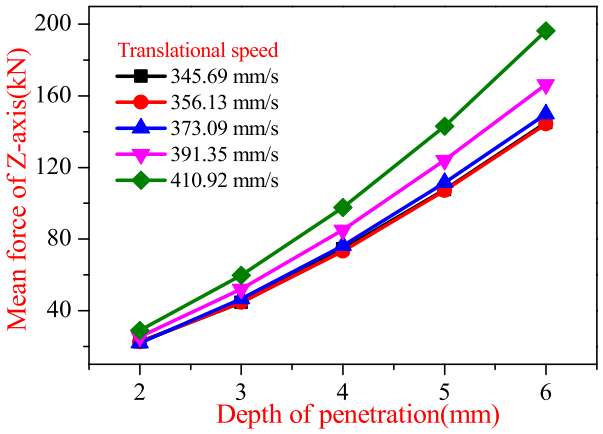

FIGURE 20. Positive force in different penetration depths.

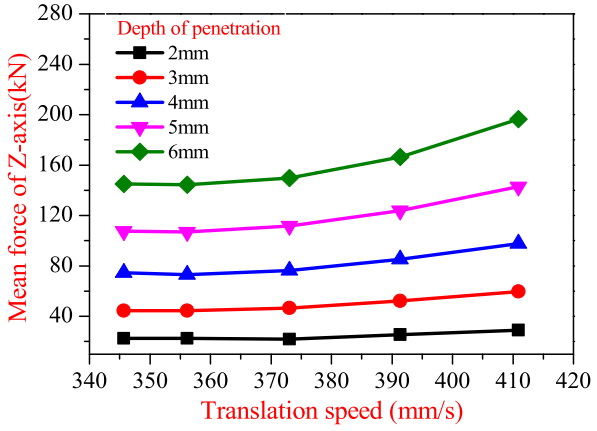

FIGURE 21. Positive force at different translation speeds.

increases; When the penetration depth is small, the positive force remains basically unchanged as the translation speed increases; when the penetration depth is large, the positive force of the hob increases slowly, as shown in the Figure 21.

At different moving speeds, the increasing trend of the positive force of the hob is linearly increased. It can be said that the feed force and the positive force increase linearly under different crushing conditions, as shown in the Figure 22.

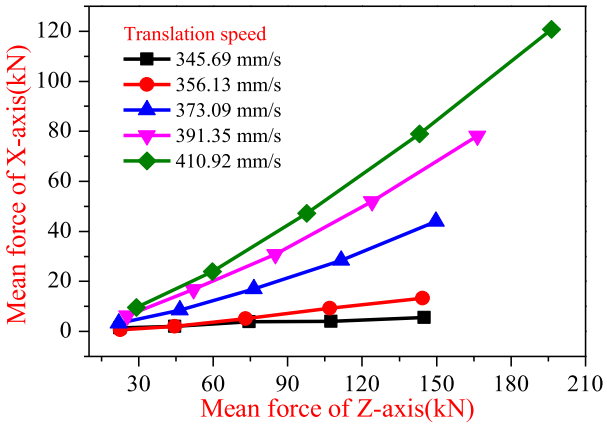

FIGURE 22. Feed force under different positive forces.

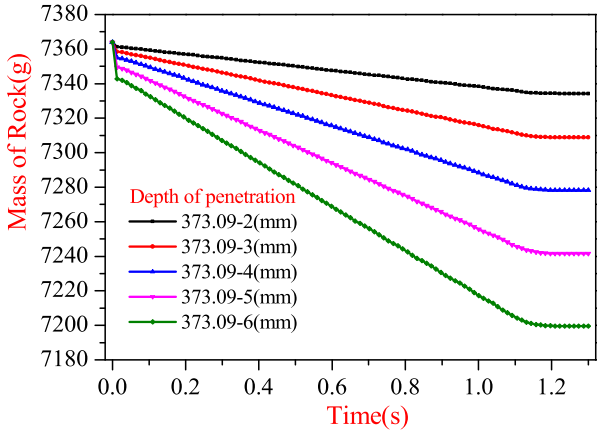

FIGURE 23. Rock fragmentation volume at different times.

C. FRAGMENTATION VOLUME

As the penetration depth of the hob increases, the volume of the rock crushing is obviously increased, and the rock crushing process is relatively uniform, which also indicates that the misalignment angle between the rows of teeth is arranged reasonably, as shown in the Figure 23.

As the translation speed of the hob increases, the volume of rock fracture firstly decreases and then increases. In different penetration depths, the volume of the fractured rock at the translation speed of 373.09 mm/s is the minimum, as shown in the Figure 24 and Figure 25.

D. FRICTION WORK

The analysis shows that the translation speed of the hob not only directly affects the force of the hob in all directions, but also directly affects the fracture state and effect of the rock. In the project, because the rock surface is uneven, the rock breaking of the hob rolls with a row or a few rows of teeth as the force point, the rotation speed and the translation speed are always in a matching state, the above five kinds of the translation speeds are likely to occur; however, in a relatively uniform rock formation, the hob can only be operated in one type. From the structure of the hob, it relies on the friction between the rocks to drive its rotation, so its actual motion

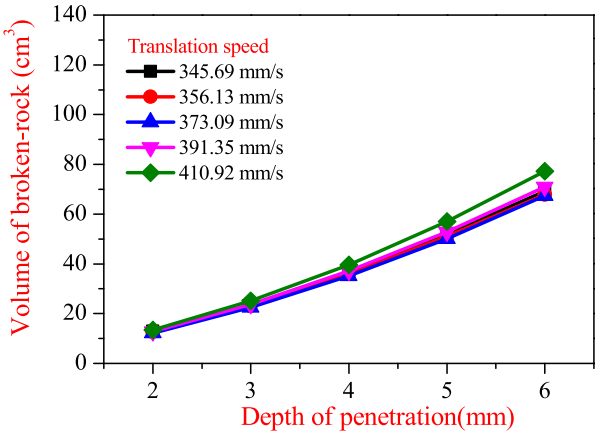

FIGURE 24. Rock fragmentation volume in different penetration depths.

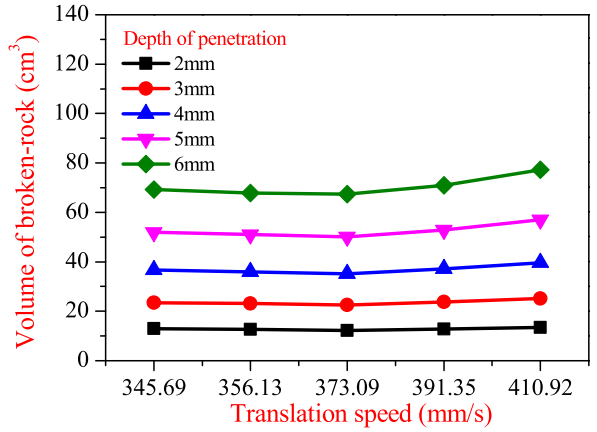

FIGURE 25. Rock fragmentation volume at different translation speeds.

state is the power consumed which is the smallest, that is, the friction work done by the actual motion state of the rock breaking by the hob.

The friction of the hob is linear with the vertical force on the rock surface, and the displacement of the frictional sliding is also linear with the volume of the rock fracture and the fracture's cross section. When the penetration depth is a constant, the friction coefficient of the rock and the cutter teeth and the ratio of the rock fracture volume to the fracture's cross section are constant, so the product of the feed force and the volume of the rock fracture volume can be used to represent the friction work of the hob. Equation 5 is shown as follows:

$$W_f = f_S^* = \mu F_\perp^* V/A = k^* F_\perp V \tag{5}$$

where: W_f represents the friction work of the cutter teeth; f is the friction force of the cutter teeth; s represents the displacement of the frictional force; μ represents the friction coefficient of the cutter teeth and the rock; $F_\perp$ represents the positive force of the rock; V represents the volume of broken rock; A represents the cross-sectional area of the rock's sliding fracture; k is a constant, and $k = \mu/A$.

It can be seen from the trend of friction work that the hob performs the minimum friction work at a speed

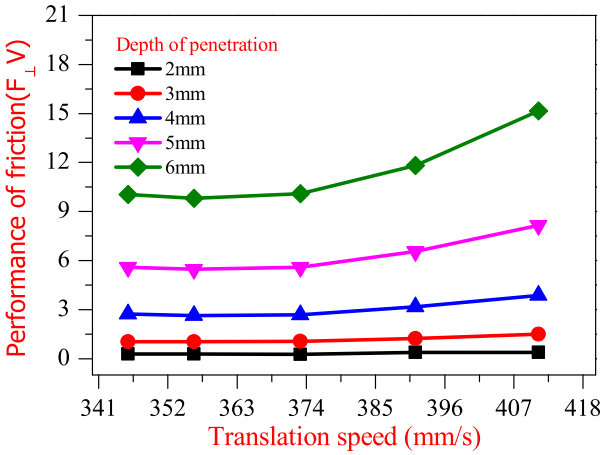

FIGURE 26. Friction work at different translation speeds.

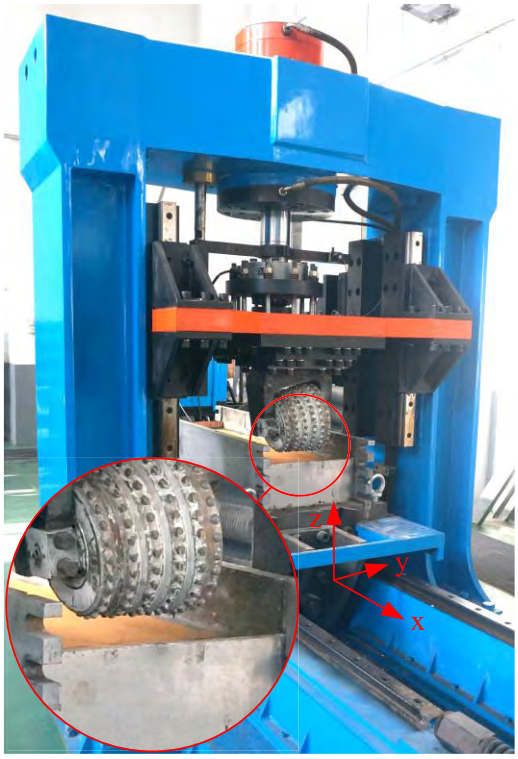

FIGURE 27. Experimental equipment for rock breaking with tipped hob cutter.

of 373.09 mm/s in different penetration depths, as shown in the Figure 26, the hob has no slip position in the third row of teeth. In view of the rock's crushing volume, it can be considered that the hob has no slip in the third row of teeth, and the two rows of teeth near the small end slide forward, and the two rows of teeth near the big end are broken rocks in a backward sliding state.

E. EXPERIMENT

In order to verify the three failure states of the tipped hob breaking rock, the experiment was carried out on the hob's broken rock, as shown in the Figure 27.

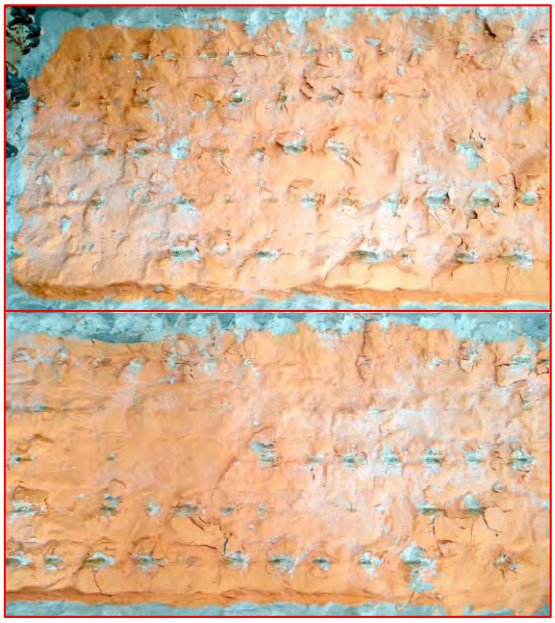

FIGURE 28. Rock surface after the tipped hob rolling.

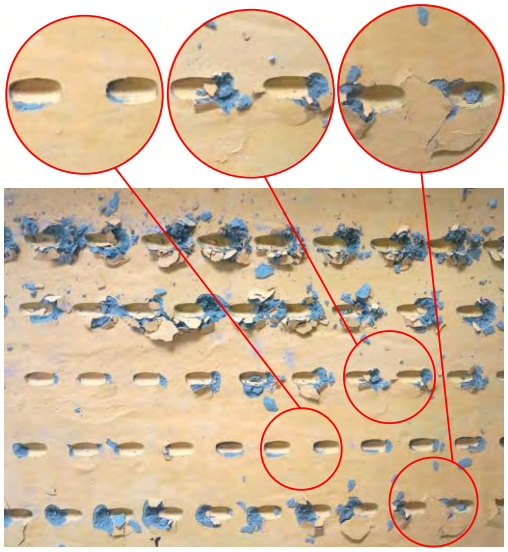

FIGURE 29. Concrete surface after the tipped hob rolling.

After the rock is broken, it is difficult to see the slip state of the teeth. Because the rock is a brittle material, the rock is easily separated from the original rock surface after being broken, making it difficult to judge the type of slip damage based on the debris. In addition, the surface of the rock is rough and uneven, and the teeth contacted at different positions are not uniform, causing some teeth unable to contact the rock, as shown in the Figure 28.

Therefore, artificial concrete was used instead of rock in the experiment, and paint was applied to the concrete to show the damaged area. The hob model used in the figure is exactly same as the simulation model. In the Figure 29 the top row of the concrete damage area represents the minimum track of the end tooth rolling. It can be clearly seen from the figure that the forward slip, the non-slip and the backward slip are significantly different in the direction of the rock failure.

IV. CONCLUSION

The motion state of the tipped hob cutter is used to establish the finite element model of the hob rolling and rock breaking. The numerical simulation method reveals the rock breaking mechanism process of the tipped hob cutter and the penetration depth of different rocks and the different broken state. The feed force, lateral force, and positive force are analyzed to find out their variation laws and correlations. Based on the above results, the main conclusions include:

1. The finite element model of rock-breaking can not only reflect the rock slip and fracture condition correctly, but also correctly reflect the change of the hob load with time, indicating the material parameter setting, meshing point, contact algorithm, etc., both of which are reasonable with the simulation results obtained by the model having higher credibility.

2. As the penetration depth increases, the feed force, lateral force and positive force of the hob obviously increase. Among them, the feed force increases linearly, while the positive force increases exponentially. In the process of rock breaking, the order of the three forces is positive force $>$ feed force $>>$ lateral force (lateral force is much smaller than the other two forces). Relative to the penetration depth, the moving speed has less influence on these kinds of forces. Therefore, in the actual engineering, while avoiding the cutter wear, the speed should be increased to improve the efficiency of the project.

3. With analyzing the motion state of the tipped hob cutter, it is proposed that when the tipped hob cutter breaks the rock, the rock damage form has three types: forward slip, no slip, and backward slip. Combined with the changing trend of a rock's crushing volume and frictional work, it is proposed that the hob moves with the minimum frictional power. The rock breaking forms include no slip in the middle, sliding forward near the small end, and sliding backwards near the big end.

REFERENCES

[1] J. Cao and S.-D. Zhao, "A fuzzy logic model to predict the specific power of rock fragmentation for large-diameter shaft rigs rolling cutters," in *Proc. IEEE Int. Conf. Mechatronics Automat.*, Xi'an, China, Aug. 2010, pp. 323–328.

[2] H. Yang, H. Wang, and X. Zhou, "Analysis on the rock–cutter interaction mechanism during the TBM tunneling process," *Rock Mech. Rock Eng.*, vol. 49, no. 3, pp. 1073–1090, Mar. 2016.

[3] Q. Geng, Z. Wei, H. Meng, and Q. Chen, "Numerical and experimental research on the rock-breaking process of tunnel boring machine normal disc cutters," *J. Mech. Sci. Technol.*, vol. 30, no. 4, pp. 1733–1745, Apr. 2016.

[4] Q. Geng, Z. Wei, H. Meng, F. J. Macias, and A. Bruland, "Free-face-assisted rock breaking method based on the multi-stage tunnel boring machine (TBM) cutterhead," *Rock Mech. Rock Eng.*, vol. 49, no. 11, pp. 4459–4472, Nov. 2016.

[5] C. Labra, J. Rojek, and E. Oñate, "Discrete/finite element modelling of rock cutting with a TBM disc cutter," *Rock Mech. Rock Eng.*, vol. 50, no. 3, pp. 621–638, Mar. 2016.

[6] J. Li, Y. Nie, K. Fu, C, Ma, J.-B. Guo, and M.-X. Xu, "Experiment and analysis of the rock breaking characteristics of disc cutter ring with small edge angle in high abrasive grounds," *J. Brazilian Soc. Mech. Sci. Eng.*, vol. 40, no. 10, p. 505, Oct. 2018.

[7] X. Li, S. Wang, R. Malekian, S. Hao, and Z. Li, "Numerical simulation of rock breakage modes under confining pressures in deep mining: An experimental investigation," *IEEE Access*, no. 4, pp. 5710–5720, 2017.
[8] D. Zhu, W. Guo, and L. Song, "TBM disc cutter model based on admissible energy principles," *Trans. Tianjin Univ.*, vol. 24, no. 2, pp. 191–200, Mar. 2018.
[9] S.-O. Choi and S.-J. Lee, "Three-dimensional numerical analysis of the rock-cutting behavior of a disc cutter using particle flow code," *KSCE J. Civil Eng.*, vol. 19, no. 4, pp. 1129–1138, May 2015.
[10] Y. Lv, H. Li, X. Zhu, and L. Tang, "Bonded-cluster simulation of rock-cutting using PFC2D," *Cluster Comput.*, vol. 20, no. 2, pp. 1289–1301, Jun. 2017.
[11] J. Rojek, "Discrete element thermomechanical modelling of rock cutting with valuation of tool wear," *Comput. Part. Mech.*, vol. 1, no. 1, pp. 71–84, May 2014.
[12] S.-O. Choi and S.-J. Lee, "Numerical study to estimate the cutting power on a disc cutter in jointed rock mass," *KSCE J. Civil Eng.*, vol. 20, no. 1, pp. 440–451, Jan. 2016.
[13] A. Mir, X. Luo, and A. Siddiq, "Smooth particle hydrodynamics study of surface defect machining for diamond turning of silicon," *Int. J. Adv. Manuf. Technol.*, vol. 88, nos. 9–12, pp. 2461–2476, Feb. 2017.
[14] X. Xiao, H. Zhu, and Y. Fan, "A 3D FEM methodology for rock breakage in rotary-percussive drilling," in *Proc. Int. Conf. Comput. Inf. Sci.*, Dec. 2010, pp. 112–115.
[15] P. L. Menezes, "Influence of cutter velocity, friction coefficient and rake angle on the formation of discontinuous rock fragments during rock cutting process," *Int. J. Adv. Manuf. Technol.*, vol. 90, nos. 9–12, pp. 3811–3827, Jun. 2017.
[16] P. L. Menezes, "Influence of rock mechanical properties and rake angle on the formation of rock fragments during cutting operation," *Int. J. Adv. Manuf. Technol.*, vol. 90, nos. 1–4, pp. 127–139, Apr. 2017.
[17] X. Liu, S. Liu, and H. Ji, "Mechanism of rock breaking by pick assisted with water jet of different modes," *J. Mech. Sci. Technol.*, vol. 29, no. 12, pp. 5359–5368, Dec. 2015.
[18] J. P. Loui and U. M. R. Karanam, "Numerical studies on chip formation in drag-pick cutting of rocks," *Geotechn. Geological Eng.*, vol. 30, no. 1, pp. 145–161, Feb. 2012.
[19] P. L. Menezes, M. R. Lovell, I. V. Avdeev, J.-S. Lin, and C. F. Higgs, "Studies on the formation of discontinuous chips during rock cutting using an explicit finite element model," *Int. J. Adv. Manuf. Technol.*, vol. 70, nos. 1–4, pp. 635–648, Jan. 2014.
[20] C. Shi, X. Zhu, and H. Luo, "Study of DTH bit–rock interaction numerical simulation method and DTH bit properties evaluation," *Arabian J. Sci. Eng.*, vol. 42, no. 5, pp. 2179–2190, May 2017.
[21] P. Samui, R. Kumar, and P. Kurup, "Determination of optimum tool for efficient rock cutting," *Geotechn. Geological Eng.*, vol. 34, no. 4, pp. 1257–1265, Aug. 2016.
[22] X. Wang, O. Su, Q.-F. Wang, and Y.-P. Liang, "Effect of cutting depth and line spacing on the cuttability behavior of sandstones by conical picks," *Arabian J. Geosci.*, vol. 10, no. 23, p. 525, Dec. 2017.

XIUKUN HU received the B.S. degree in mechanical engineering from Jinan University, Jinan, Shandong, China, in 2009, and the M.S. degree in mechanical engineering from the Shandong University of Science and Technology, Qingdao, Shandong, China, in 2012. He is currently pursuing the Ph.D. degree in mechanical engineering with the China University of Mining and Technology, Xuzhou, Jiangsu, China. Since 2012, he has been involved in the design of coal mine machinery products with Shandong Tai'an Coal Mining Machinery Company, Ltd. His research interests include the reliability of steel structures and the fragmentation of hard rock based on FE simulation.

CHANGLONG DU was born in Peixian, Jiangsu, in 1958. He received the M.S. degree in mechanical engineering and the Ph.D. degree in mining engineering from the China University of Mining and Technology, Xuzhou, Jiangsu, China, in 1987 and 1994, respectively. From 1994 to 2000, he served as the Director and the General Branch Secretary with the China University of Mining and Technology Machinery. Since 2001, he has been with the School of Mechanical and Electrical Engineering, China University of Mining and Technology, where he is currently a Professor and a Doctoral Supervisor. He holds seven national invention patents and 25 utility model patents and has published four monographs and more than 110 academic papers.

SONGYONG LIU was born in 1981. He received the Ph.D. degree from the China University of Mining and Technology, China, in 2009, where he is currently a Professor with the School of Mechatronic Engineering. His research interests include the design and dynamics of excavation machinery, and rock breaking assisted with water jet.

HAO TAN was born in 1987. He received the B.S. degree from the Hefei University of Technology and the M.S. degree from the General Institute of Coal Science. He is currently pursuing the Ph.D. degree in civil engineering with the Beijing University of Science and Technology, Beijing, China. He has participated in rock mechanics including laboratory and field tests and the fragmentation of hard rock based on FE simulation.

ZHIQIANG LIU was born in 1962. He is currently the Chief Scientist of China Coal Science and Technology Group Company, Ltd., the Vice President of the Tiandi Science and Technology Wells Construction Research Institute, and the Chief Engineer of Beijing China Coal Mine Engineering Company, Ltd. His main research direction is the design of deep well equipment. He has participated in the design of LM-90, LM-120, LM-200, and other types of raise boring rigs in China.